

# Strengthening of Tropical Indian Ocean Teleconnection to the Northwest Pacific since the Mid-1970s: An Atmospheric GCM Study\*

GANG HUANG

*LASG, Institute of Atmospheric Physics, Chinese Academy of Sciences, Beijing, China*

KAIMING HU

*LASG, Institute of Atmospheric Physics, and Graduate University of the Chinese Academy of Sciences, Beijing, China*

SHANG-PING XIE

*International Pacific Research Center, and Department of Meteorology, University of Hawaii at Manoa, Honolulu, Hawaii*

(Manuscript received 15 December 2009, in final form 21 April 2010)

## ABSTRACT

The correlation of northwest (NW) Pacific climate anomalies during summer with El Niño–Southern Oscillation (ENSO) in the preceding winter strengthens in the mid-1970s and remains high. This study investigates the hypothesis that the tropical Indian Ocean (TIO) response to ENSO is key to this interdecadal change, using a 21-member ensemble simulation with the Community Atmosphere Model, version 3 (CAM3) forced by the observed history of sea surface temperature (SST) for 1950–2000. In the model hindcast, the TIO influence on the summer NW Pacific strengthens in the mid-1970s, and the strengthened TIO teleconnection coincides with an intensification of summer SST variability over the TIO. This result is corroborated by the fact the model's skills in simulating NW Pacific climate anomalies during summer increase after the 1970s shift.

During late spring to early summer, El Niño–induced TIO warming decays rapidly for the epoch prior to the 1970s shift but grows and persists through summer for the epoch occurring after it. This difference in the evolution of the TIO warming determines the strength of the TIO teleconnection to the NW Pacific in the subsequent summer. An antisymmetric wind pattern develops in spring across the equator over the TIO, and the associated northeasterly anomalies aid the summer warming over the north Indian Ocean by opposing the prevailing southwest monsoon. In the model, this antisymmetric spring wind pattern is well developed after but absent before the 1970s shift.

## 1. Introduction

The northwest Pacific (NWP) summer monsoon is an important component of the Northern Hemisphere summer monsoon (Murakami and Matsumoto 1994; Ueda and Yasunari 1996; Ueda et al. 2009; Wu and Wang 2000). Year-to-year variations of the NWP monsoon significantly affect the occurrence of the flooding–drought

events over East Asia (Huang and Wu 1989; Chang et al. 2000) via the Pacific–Japan teleconnection pattern (Nitta 1987; Kosaka and Nakamura 2006; Arai and Kimoto 2008). Interannual variability in the NWP summer monsoon is correlated with El Niño–Southern Oscillation (ENSO) in the preceding winter (Wang et al. 2003). In the summer following El Niño, rainfall decreases over the subtropical NWP with an anomalous anticyclone near the surface. In East Asia, summer rainfall tends to be excessive.

ENSO-induced SST anomalies persist through summer over the tropical Indian Ocean (TIO; Du et al. 2009). They have been implicated as anchoring summer climate anomalies over the NWP and East Asia via the so-called capacitor effect (Yang et al. 2007; Li et al. 2008). Xie et al. (2009) show that atmospheric Kelvin waves are

---

\* International Pacific Research Center Publication Number 704 and School of Ocean and Earth Science and Technology Publication Number 7093.

---

Corresponding author address: Gang Huang, LASG, IAP, CAS, P.O. Box 9804, Beijing 100029, China.  
E-mail: hg@mail.iap.ac.cn

the key bridge between the TIO and subtropical NWP. El Niño-induced TIO swarming force a Matsuno (1966)–Gill (1980) pattern in tropospheric temperature. The warm tropospheric Kelvin wave propagates into the western Pacific, inducing Ekman divergence in the subtropical NWP to suppress convection and develop an anticyclonic circulation near the surface. Recent forecast experiments using a coupled general circulation model (GCM) confirm this TIO teleconnection to the NWP (Chowdary et al. 2010).

The correlation between the NWP monsoon and ENSO has apparently strengthened since the mid-1970s, possibly related to the enhanced ENSO variance (Wang et al. 2008). An observational study by Xie et al. (2010) suggests that this interdecadal change originates in changes in the TIO teleconnection to the NWP. The El Niño-induced TIO warming takes place during epochs both before and after the mid-1970s shift, but it persists into summer only after the mid-1970s. Accordingly, the tropospheric Kelvin wave it forces strengthens substantially in the postshift epoch.

The earlier-mentioned observational studies suggest a strengthening of the TIO teleconnection to the NWP, which seems to explain the apparent increase in correlation of NWP summer monsoon variability with ENSO two seasons in advance. Given that TIO SST anomalies are an important source of summer climate predictability over the NWP and East Asia (Chowdary et al. 2010), it is important to investigate the cause of the interdecadal change in the TIO teleconnection. While increased ENSO activity (Wang et al. 2008) and enhanced TIO SST variability (Xie et al. 2010) are a plausible cause, alternative explanations cannot be ruled out from observations alone. For example, improvements in observations and their assimilation into reanalysis products reduce sampling errors and may lead to an apparent increase in correlation, or chaotic variability in the atmosphere can also cause apparent variations in correlation.

The present study examines the cause of the apparent strengthening of the TIO teleconnection to the summer NWP based on a 21-member ensemble simulation using an atmospheric general circulation model (AGCM) forced by observed SST for 1950–2000. The AGCM ensemble simulation reproduces the interdecadal change similar to observations. We then proceed to examine interdecadal change in TIO SST response to ENSO and its subsequent influence on the NWP. The enhanced persistence of TIO SST anomalies since the mid-1970s is related to a change in wind pattern in the preceding season.

The rest of the paper is organized as follow. Section 2 describes the data and numerical simulation. Section 3 reviews observational evidence for the interdecadal

change in the TIO teleconnection. Sections 4 and 5 diagnose the model output, examining the interdecadal change during boreal summer and spring, respectively. Section 6 is a summary.

## 2. Data and model

We use the Met Office Hadley Centre Sea Ice and SST (HadISST) dataset (Rayner et al. 2003) and the National Centers for Environmental Prediction (NCEP) atmospheric reanalysis (Kalnay et al. 1996), originally on  $1^\circ$  and  $2.5^\circ$  grids, respectively. Our study focuses on interannual variability. Except in the wavelet analysis, a linear trend has been subtracted from raw anomalies to remove decadal and longer variations.

SST anomalies averaged over the region of  $10^\circ\text{S}$ – $20^\circ\text{N}$ ,  $40^\circ$ – $100^\circ\text{E}$  are used as an index for TIO SST variations, and the meridional difference of 850-hPa zonal wind anomalies between a southern region ( $5^\circ$ – $15^\circ\text{N}$ ,  $100^\circ$ – $130^\circ\text{E}$ ) and a northern region ( $20^\circ$ – $30^\circ\text{N}$ ,  $110^\circ$ – $140^\circ\text{E}$ ) is used as an index for the NWP summer anticyclone, following the NWP summer monsoon index by Wang et al. (2001), but with the sign reversed. Both indices are defined for boreal summer [June–August (JJA)]. Hereafter, seasons refer to those for the Northern Hemisphere.

We use the Community Atmosphere Model, version 3 (CAM3) at T42 resolution (equivalent to  $2.8^\circ$  latitude  $\times$   $2.8^\circ$  longitude) in the horizontal and 23 sigma levels in the vertical. Details of the models are provided in Collins et al. (2006). A 21-member ensemble of CAM3 simulations are performed with HadISST observations as surface boundary conditions for a 51-yr period of 1950–2000. Each member simulation differs only in the initial conditions.

## 3. Observed interdecadal change in TIO teleconnection

This section presents results from an observational analysis to be compared with the AGCM hindcast. Figure 1 shows the correlation in 15-yr sliding windows between JJA TIO SST and NWP anticyclone indices (solid line). The correlation is weak ( $-0.4$  to  $0.1$ ) and insignificant for the first half of the record and rises dramatically in the mid-1970s. It peaks above 0.8 in 1980 and somewhat decreases afterward but stays above the 95% significance level for the past three decades. The strengthening in the mid-1970s of this TIO teleconnection to the NWP is the focus of this study. A weakening is also seen in the WNP anticyclone–TIO SST relationship in the mid-1990s, which may be related to the decadal change in the East Asian summer monsoon as studied by Kwon et al. (2005).

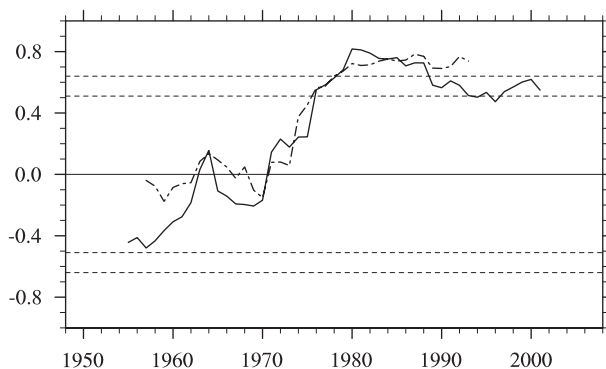


FIG. 1. The 15-yr sliding correlation between the NWP anticyclone and JJA TIO SST indices of observation (solid line), and for the NWP anticyclone index between observations and the ensemble-mean simulation (dot-dash line). Horizontal black dash lines denote 95% and 99% confidence levels.

To document the interdecadal change, we partition the data into preshift (PRE) and postshift (POST) periods of 1953–76 and 1977–2000, respectively. Figure 2 compares the correlations of SST, 850-hPa wind velocity, and tropospheric (850–200-hPa mean) temperature with the NWP anticyclone index between the PRE and POST epochs. During the POST epoch, positive SST correlation is found over the north TIO through the South China Sea. In response to the TIO warming, troposphere temperature displays a Matsuno–Gill pattern with the maximum correlation over the eastern TIO. A Kelvin wave wedge penetrates the western Pacific along the equator, with a pronounced anticyclonic circulation on its northern flank. These results are consistent with the Kelvin wave–induced Ekman divergence mechanism of Xie et al. (2009) for the NWP anticyclone. During the PRE epoch, SST correlation with the NWP anticyclone is weak, except over small patches off Sumatra, in the South China Sea and NWP. SST correlation features an east–west contrast in the TIO, with negative values in the western TIO and westerly wind anomalies on the equator. Consistent with weak SST anomalies, there is no significant tropospheric temperature correlation over the TIO. The NWP anticyclone correlation with the concurrent summer Niño-3.4 SST index is low,  $-0.41$  and  $-0.11$  for the PRE and POST epochs, respectively. These results support that the TIO influence on the NWP anticyclone is weak prior to the mid-1970s and strengthens afterward.

Figure 3 shows wavelet spectra of summer TIO SST and NWP anticyclone indices. In a frequency band of approximately four years, TIO SST variability experienced a prominent increase in the late 1970s (Fig. 3a). There is a concurrent increase in NWP anticyclone variability in the same frequency band (Fig. 3b). Moreover, both TIO SST

and NWP anticyclone variability displays a concurrent shift in dominant frequency from 4 to 3 yr in the 1990s. All this suggests TIO SST and its teleconnection as the cause of intensified variability in the NWP anticyclone. This hypothesis is consistent with the earlier-mentioned correlation analysis and will be tested with the CAM hindcast.

#### 4. Summer interdecadal change in model

We first evaluate model skills by performing the empirical orthogonal function (EOF) analysis for ensemble-mean variability in JJA 850-hPa wind velocity over the NWP. Figure 4 compares the leading EOF modes with observations. In observations, the first mode explains 28% of the total variance, featuring an anticyclone associated with positive sea level pressure (SLP) anomalies over the subtropical NWP (Fig. 4, upper left). The second mode explains 16% of the variance, featuring westerly anomalies along the equator with zonal SLP gradient. There is a weak subtropical anticyclone over East Asia and the NWP (Fig. 4, lower left). Correlation analysis with eastern Pacific SST indicates that the second EOF (EOF-2) represents anomalies during the summer when El Niño develops [JJA(0)] and EOF-1 represents the summer after El Niño decays [JJA(1)]. Here the numerals in parentheses denote the El Niño developing (0) and decay (1) years. The first principal component (PC-1) is highly correlated with the NWP anticyclone index at  $r = 0.92$ .

The model ensemble-mean simulation captures the salient features of observed EOFs with the following differences: 1) the model EOF-1 explains a much larger fraction of variance possibly because of weaker noise than in observations; 2) the anticyclone in the model EOF-1 is shifted by  $5^\circ$  northward; and 3) in the model EOF-2, the subtropical anticyclone is confined to East Asia and the off-equatorial low-pressure belt to the south is more pronounced.

Figure 5 shows the 15-yr sliding correlation for PCs between observations and the ensemble mean. While the PC-2 correlation remains nearly constant and above the 95% significance level throughout, the model's skills in PC-1 displays a pronounced interdecadal change in the late 1970s, low and insignificant before the shift but rising rapidly afterward to values as high as 0.7. The ensemble-mean AGCM simulation helps isolate the SST-forced variability (Rowell et al. 1995; Lu et al. 2006). The high correlation for the NWP EOF-1 mode between observations and the ensemble-mean simulation during the POST epoch (Fig. 5) indicates that the year-to-year variations in the NWP summer monsoon are forced by SST anomalies, while the low correlation suggests that the SST forcing is weak during the PRE

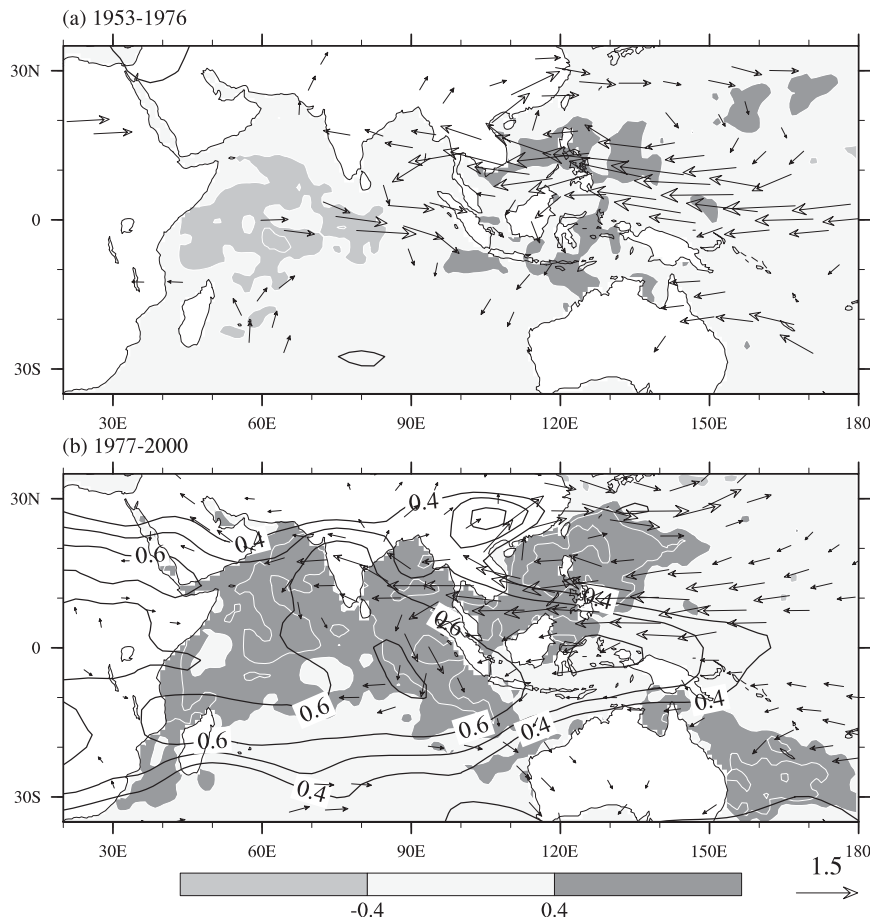


FIG. 2. Correlation with the NWP anticyclone index in observation during (a) 1953–76 and (b) 1977–2000: JJA SST (gray shade and white contours at intervals of 0.2) and tropospheric temperature (vertical average from 850 to 200 hPa; contours  $r \geq 0.4$ ). Wind vectors ( $\text{m s}^{-1}$ , pass the 95% confidence level) show the regression of 850-hPa wind with the NWP anticyclone index.

epoch. Thus, it is possible that changes in SST patterns cause this interdecadal change.

Indeed, the model simulates the late 1970s' increase in interannual variability of the NWP anticyclone (Fig. 3c), even the shift of the dominant frequency from 4–5 to 3 yr. The concurrent increase in TIO SST variability suggests it as the cause of enhanced NWP anticyclone variability. NWP anticyclone variability may be due to internal variability or forced by SST anomalies (Lu et al. 2006). Ensemble AGCM simulations capture only SST-forced variability, which appears to dominate the NWP anticyclone after the mid-1970s. Figure 5 shows that the rise of the model's skills in simulating NWP climate anomalies coincides with the increase in observed correlation between TIO SST and NWP anticyclone variability (Fig. 2).

#### *TIO teleconnection*

The rest of the section examines the TIO teleconnection to the NWP. Figure 6 compares the correlation between

the TIO SST and NWP anticyclone in 21 simulations with CAM3. A total of 12 members out of 21 show the correlation exceeding the 95% confidence level during the POST epoch, but none passes the 95% confidence level during the PRE epoch. Moreover, the correlation coefficients are higher during the POST epoch than the PRE epoch in every member of the simulations, illustrating the strengthened TIO teleconnection after the mid-1970s.

Figure 7 compares summer correlations of ensemble-mean precipitation, tropospheric temperature, and 850-hPa wind with TIO SST between the PRE and POST epochs. Consistent with observations during the POST epoch, a TIO warming forces a Matsuno–Gill pattern in tropospheric temperature, with a warm Kelvin wave propagating into the western Pacific along the equator and Rossby wavelike off-equatorial maxima over the western TIO and Africa. Precipitation increases over the TIO except over the Bay of Bengal. A low-level anticyclone

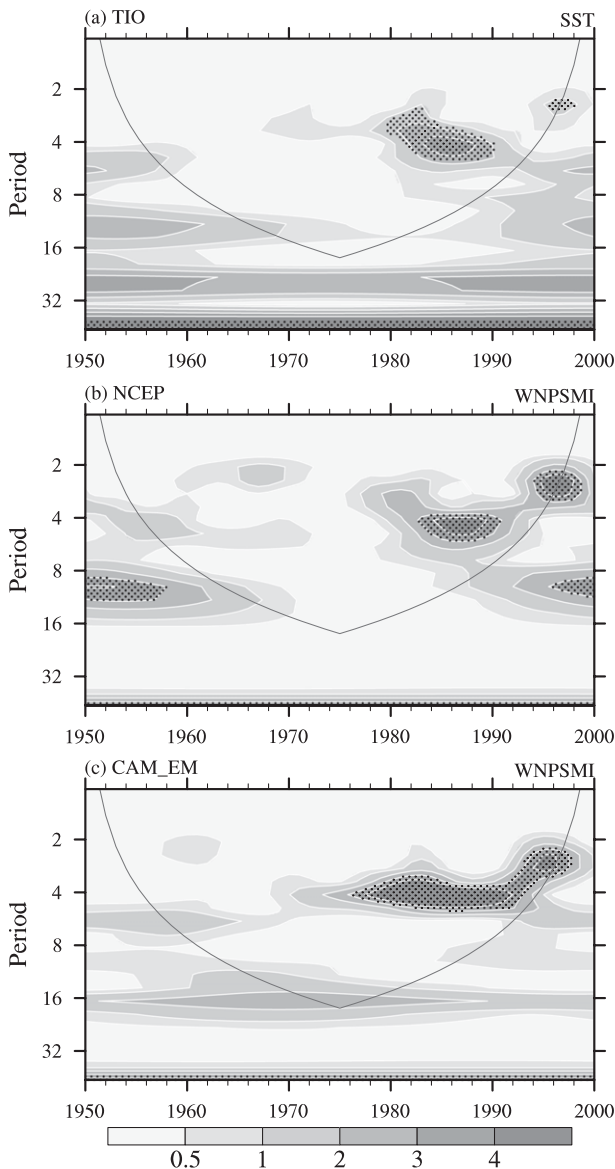


FIG. 3. Wavelet spectra of the standard deviation of the (a) JJA TIO SST index, (b) observations NWP anticyclone index, and (c) ensemble-mean NWP anticyclone index. All shaded regions denote 95% confidence levels.

appears on the northern flank of the tropospheric Kelvin wave from the Bay of Bengal to the subtropical WNP, where precipitation shows a tendency to decrease. During the PRE epoch, by contrast, the Matsuno–Gill pattern weakens over the TIO, without the development of the warm Kelvin wave in the equatorial western Pacific and anticyclonic anomalies over the NWP. Over the central Pacific, a pair of warm anomaly maxima develops in tropospheric temperature on either side of the equator. The cause of these off-equatorial maxima in tropospheric warming needs further investigation.

These results from the model hindcast indicate that the increase in TIO SST variability strengthens its influence on NWP climate. They support the notion that the warm tropospheric Kelvin wave is a key element of this teleconnection.

### 5. Antisymmetric wind pattern in spring and early summer

What caused the increase in TIO SST variability in summer after the mid-1970s? Previous studies show that El Niño induces TIO warming through atmospheric bridge (Alexander et al. 2002; Schott et al. 2009). Ocean Rossby waves are important over the southwest TIO (Xie et al. 2002; Huang and Kinter 2002), and surface heat flux adjustments dominate the rest of the TIO (Klein et al. 1999; Lau and Nath 2003).

Figure 8 shows the observed correlations with the December–February (0) [DJF(0)] Niño-3.4 SST index of SST and 850-hPa wind velocity averaged zonally over the TIO ( $40^{\circ}$ – $100^{\circ}$ E). El Niño-induced SST warming persists long over the TIO, with the correlation staying above 0.6 through JJA(1) during the POST epoch but falling below this level before June(1) in the PRE epoch. During the POST epoch, an equatorially antisymmetric wind pattern develops in March and persists through June (Kawamura et al. 2001; Wu et al. 2008). Over the North Indian Ocean (NIO), the associated easterly wind anomalies act to warm SST after the onset of the southwest monsoon by reducing the prevailing winds and surface evaporation (Du et al. 2009). Over the NIO, the easterly wind anomalies during May–July explain the peculiar SST warming that grows after El Niño has already dissipated. During the PRE epoch, the antisymmetric wind pattern does not appear in spring, and wind anomalies are weak afterward over the NIO, where SST anomalies decay rapidly (Fig. 10a).

The model reproduces observed wind anomalies quite well for the POST epoch (Fig. 9b), including the antisymmetric wind pattern during March–May(1) [spring; MAM(1)]. In both observations and the model, easterly anomalies appear in a broad equatorial band during January–March and then gradually move northward and persist over the NIO through June and July. The easterly anomalies during May–July sustain the NIO warming, and their successful simulation in our AGCM hindcast indicate that they are forced by SST anomalies—most likely those over the southwest TIO (Du et al. 2009). Indeed, positive precipitation anomalies are found over the southwest TIO during both MAM(1) (Fig. 10b) and JJA(1) (Fig. 7b). The zonal-mean wind anomalies in the model do not correlate very well with observations for the PRE epoch (Fig. 9a)—the model winds are even westerly over the NIO during JJA(1).

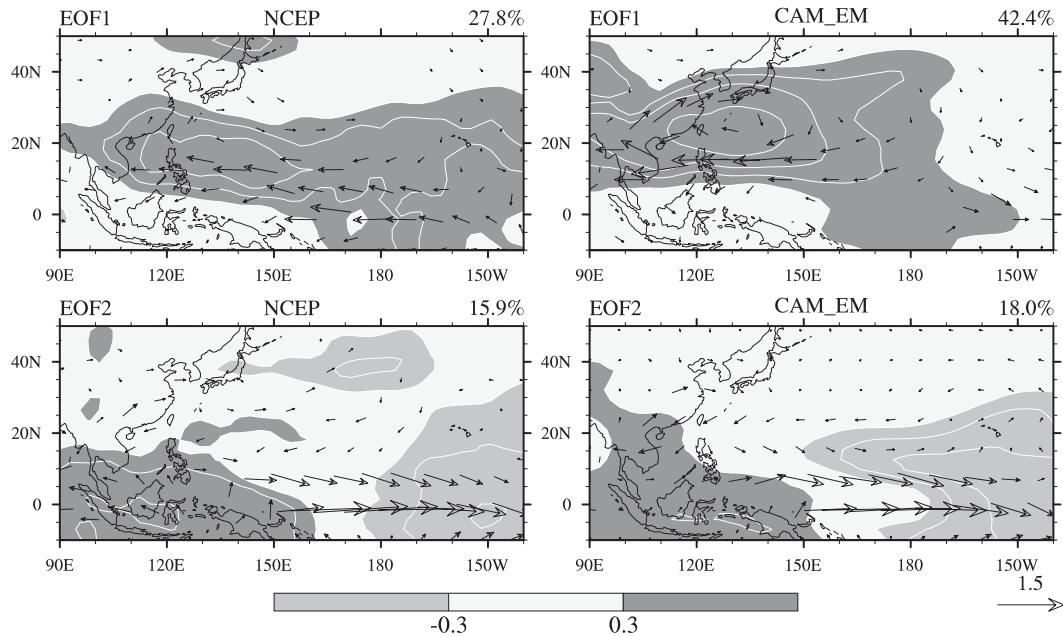


FIG. 4. Correlation of 850-hPa wind vectors and sea surface pressure in JJA with the leading PCs of 850-hPa wind velocity in (left) observations and (right) the ensemble-mean simulation: (top) EOF-1 and (bottom) EOF-2. The domain for EOF analysis covers the NWP ( $5^{\circ}$ – $50^{\circ}$ N,  $90^{\circ}$ – $180^{\circ}$ E).

Figure 10 compares the leading EOF mode for MAM 850-hPa wind velocity and associated precipitation anomalies between the PRE and POST epochs in the model. As in summer, the model skills in MAM wind simulation are low before but high after the 1970s shift (the PC-1 correlation between the hindcast and observations changes from  $-0.1$  to  $0.68$ ). During the POST epoch, EOF-1 explains a large fraction (42%) of the total variance, featuring an antisymmetric wind pattern with anomalous northeasterlies over the NIO. The associated precipitation anomalies are rough out of phase north

and south of the equator, consistent with the result of Wu et al. (2008) that the leading precipitation EOF for spring is antisymmetric about the equator. The reduced rainfall north of the equator is accompanied by anticyclonic circulation, with easterlies over the NIO. A blob of positive rainfall anomalies is found over the southwest TIO, accompanied by cyclonic circulation. Over the southwest TIO, the slow propagation of downwelling ocean Rossby waves induces SST warming and intensifies atmospheric convection, thereby forcing the antisymmetric wind pattern across the equator (Xie et al. 2002; Annamalai et al. 2005; Du et al. 2009).

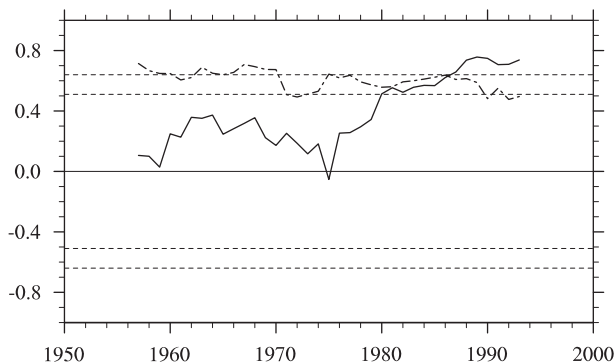


FIG. 5. Correlation between observations and the ensemble-mean simulation in 15-yr sliding windows for the first (solid line) and second (dash) PCs of JJA 850-hPa wind over the NWP. Horizontal black dash lines denote 95% and 99% confidence levels based on  $t$  test.

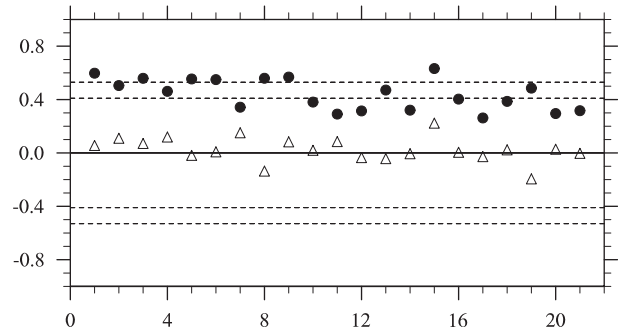


FIG. 6. Correlation coefficients between the JJA TIO SST and NWP anticyclone indices in the 21-member simulations during 1977–2000 (black circles) and 1953–76 (triangles). Horizontal dash lines denote 95% and 99% confidence levels.

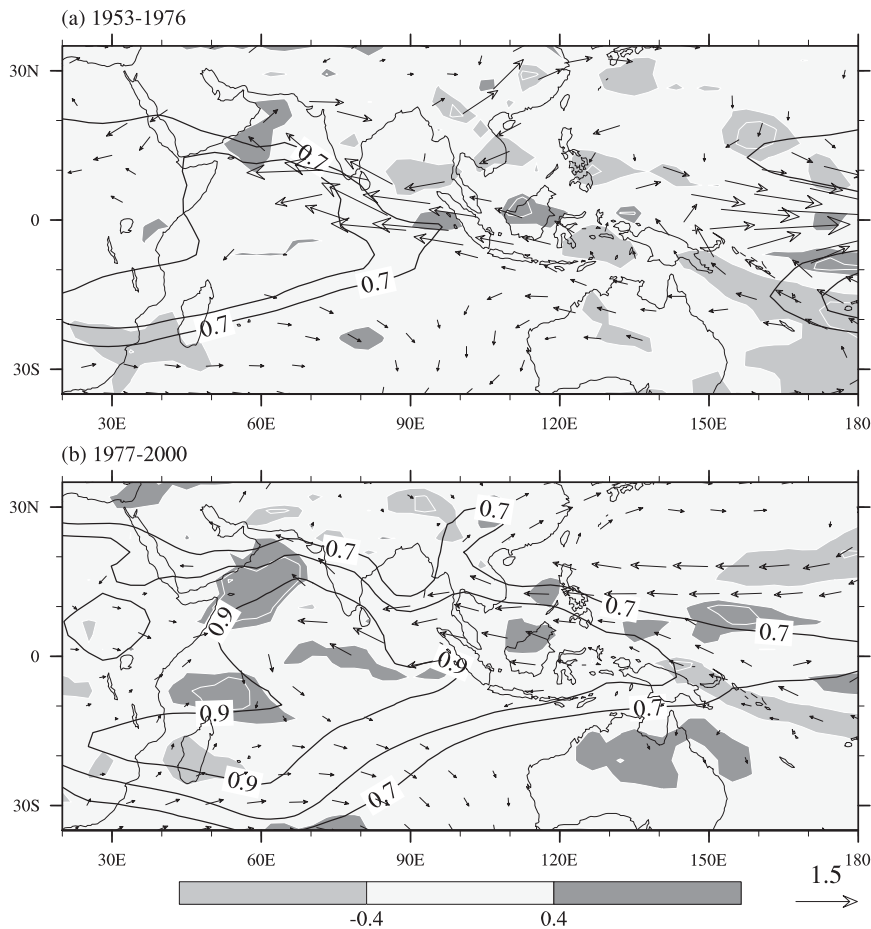


FIG. 7. As in Fig. 2, but for correlation with the JJA TIO index and ensemble-mean precipitation (gray shade and white contours at intervals of 0.2).

For the PRE epoch, EOF-1 explains a smaller fraction (33%) of variance and features easterly wind anomalies centered on the equator (Fig. 10a). The wind anomalies are consistent with a slowdown of the Walker circulation and resemble the wind pattern forced by remnant SST anomalies of a decaying El Niño (Annamalai et al. 2005). Precipitation anomalies are weak over the southwest TIO, consistent with the notion that they anchor the antisymmetric wind pattern across the equator.

Figure 11 shows the evolution of SST correlation with the model PC-1 for ensemble-mean MAM wind, to identify the SST forcing. From December to May, SST warming takes place over the entire TIO for the PRE epoch but is weak over the NIO for the POST epoch. Wu et al. (2008) suggest that the meridional SST gradient is important for the antisymmetric wind pattern, in line with wind–evaporation–SST (WES) feedback (Xie and Philander 1994). The TIO warming decays rapidly from June onward for the PRE epoch but persists through JJA for the POST epoch.

The TIO wind EOF-1 pattern for MAM is associated with Pacific SST anomalies indicative of El Niño. The evolution of Pacific SST correlation, however, is very different between the PRE and POST epochs. El Niño decays earlier during the PRE than the POST epoch. During the POST epoch, the slower decay of El Niño applies teleconnective forcing longer on the TIO, making the southwest TIO warming stronger and persist longer (Xie et al. 2010). The stronger SST forcing over the southwest TIO helps induce and persist the antisymmetric wind pattern, causing the NIO to warm during May–July. Positive SST anomalies over the southwest TIO have another effect of delaying the onset of the Indian summer monsoon, which may help sustain the NIO warming with increased solar radiation and reduced wind (Joseph et al. 1994; Annamalai et al. 2005).

For the POST epoch, we note a well-organized band of negative SST correlation over the subtropical NWP from December to May, conducive to forming a surface anticyclone (Wang et al. 2003). The NWP anticyclone

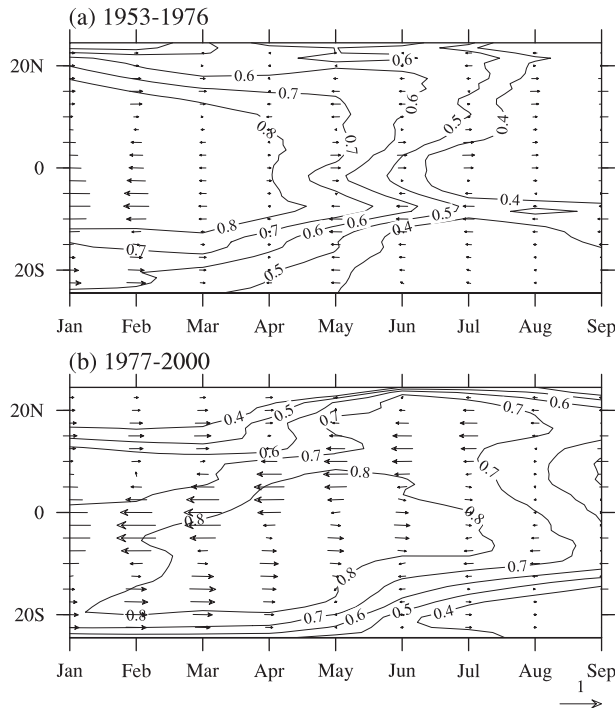


FIG. 8. Observed correlation (contours) between zonal-mean TIO SST ( $40^{\circ}$ – $100^{\circ}$ E) and the DJF Niño-3.4 index, and regression (vector) of zonal-mean 850-hPa wind upon the Niño-3.4 index during (a) 1953–76 and (b) 1977–2000, as a function of calendar month and latitude.

may propagate westward into the NIO as an atmospheric Rossby wave, helping to suppress atmospheric convection there (Kawamura et al. 2001). This suggests that the NWP cooling may serve as a remote forcing for the antisymmetric wind pattern over the TIO.

## 6. Summary and discussion

The present study has investigated interdecadal change in the relationship between TIO SST and the NWP summer anticyclone using both observations and AGCM simulations. Observations show that the NWP anticyclone is negatively correlated with summer TIO SST after the mid-1970s, but the relationship is weak for the period of 1958–76. A 21-member ensemble AGCM hindcast reproduces this interdecadal change. Together, our observational and model results show that the TIO teleconnection to the NWP strengthens after the mid-1970s, most likely as a result of enhanced variability in summer TIO SST.

Our AGCM hindcast confirms that the interannual TIO warming excites a warm tropospheric Kelvin wave and that this Kelvin wave is instrumental in inducing summer climate anomalies over the subtropical NWP,

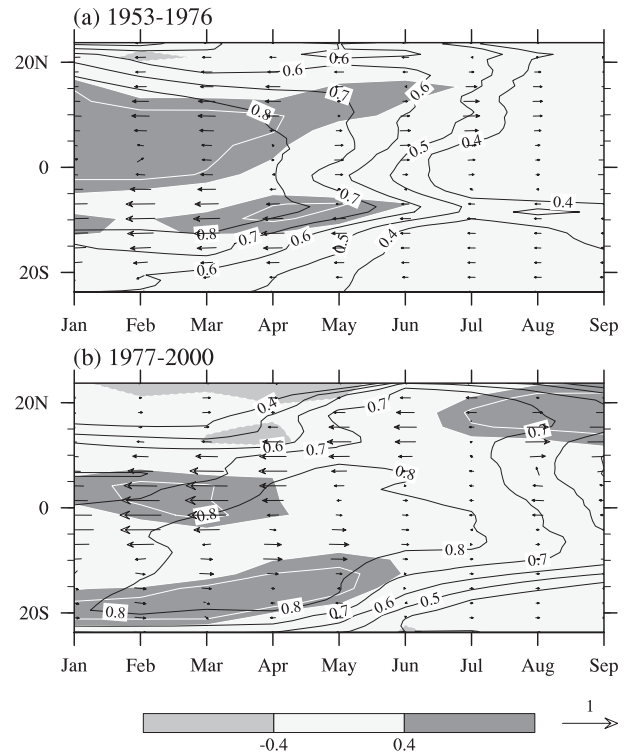


FIG. 9. As in Fig. 8, but for the ensemble-mean simulation. Superimposed is the correlation between zonal-mean ( $40^{\circ}$ – $100^{\circ}$ E) precipitation (gray shade and white contours at intervals of 0.2) and the Niño-3.4 index.

including suppressed convection and an anomalous surface anticyclone. The model captures the pronounced Kelvin wave response of the troposphere to the El Niño-induced TIO warming for the POST epoch, but the Kelvin wave response is weak for the PRE epoch, explaining weak correlation between TIO SST and NWP climate anomalies. The strong (weak) TIO teleconnection coincides with high (low) SST variability over the summer TIO on one hand and with the period when the model skills are high (low) in simulating NWP circulation anomalies on the other.

An antisymmetric wind pattern develops in spring and persists through June, likely anchored by the positive SST and precipitation anomalies in the southwest TIO. With northeasterlies north of the equator opposing the mean southwest monsoon, this wind pattern is instrumental in the summer peak of the NIO warming (Du et al. 2009). This antisymmetric spring wind pattern is captured for the POST epoch but absent in the PRE epoch in the model. The SST correlation analysis suggests that stronger meridional SST gradients during the POST epoch rather than the PRE epoch contributes to the formation of this wind pattern, and so does the slower decay of El Niño SST anomalies in the Pacific.

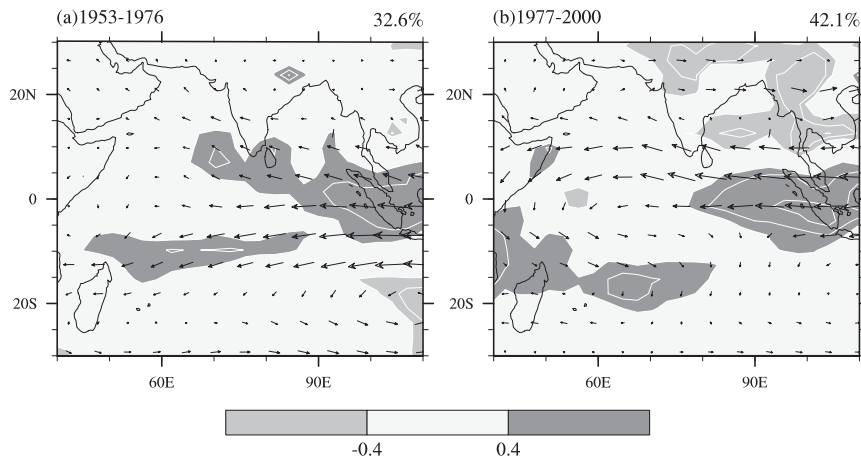


FIG. 10. First EOF modes of MAM 850-hPa wind velocity (vectors) over the TIO during (a) 1953–76 and (b) 1977–2000, with MAM precipitation correlation superimposed (gray shades and white contours at intervals of 0.2). The results are based on the ensemble-mean simulation.

Our AGCM hindcast prescribes observed SST, but SST anomalies could be interactive with wind anomalies. For example, the easterly wind anomalies and SST warming over the NIO may interact with each other: The NIO warming induced the NWP anticyclone and easterly anomalies over the Bay of Bengal–South China Sea as simulated in our hindcast (Fig. 7b) as these wind anomalies cause the ocean to warm (Du et al. 2009).

Results from our AGCM hindcast show that the interdecadal strengthening of both the antisymmetric spring wind pattern over the TIO and summer TIO teleconnection is due to changes in the pattern and magnitude of TIO SST anomalies. Such changes in TIO SST

anomalies, in turn, appear to trace back to those in ENSO in the Pacific. TIO SST anomalies are interactive with the atmosphere and with Pacific SST via atmospheric bridge [see Schott et al. (2009) for a recent review]. The interdecadal change in ENSO and its interaction with the TIO needs to be studied from a coupled ocean–atmospheric perspective.

Two strong El Niño events happened after the mid-1970s: 1982/83 and 1997/98. We have computed the correlation coefficient between the TIO SST and NWP summer anticyclone indices during 1977–2000 by excluding the years of 1983 and 1998. The correlation coefficients drop to 0.49 and 0.41 for observations and the

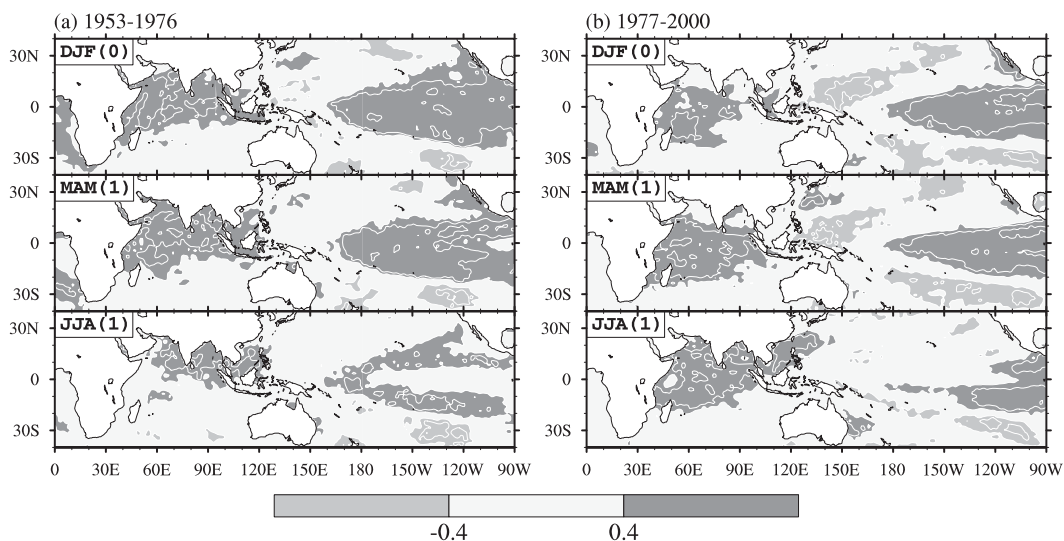


FIG. 11. Correlation of SST (gray shades and white contours at intervals of 0.2) with the first PC of MAM 850-hPa wind over the TIO from DJF to JJA during (a) 1953–76 and (b) 1977–2000.

model ensemble mean, respectively. They are lower than using the original time series (0.63 and 0.55 for observations and the simulation, respectively) but are still much higher than the correlation for the PRE epoch (Fig. 2). Thus, individual El Niño events can influence the relationship between the NWP summer monsoon and the Indian Ocean to some extent, but the sharp interdecadal change remains without the 1982/83 and 1997/98 events. The result does illustrate, however, the need to study low-frequency variations in ENSO properties.

*Acknowledgments.* The authors are grateful to Prof. Ronghui Huang and Dr. Renguang Wu for their insightful comments that led to a significant improvement of the manuscript. GH and KH are jointly supported by the National Key Technology R&D Program 2008BAK50B02 and the Natural Science Foundation of China under Grants 40890155, 40775051, and U0733002, and Project KZCX2-YW-220 CAS. S.-P. Xie is supported by the U.S. National Science Foundation and the Japan Agency for Marine-Earth Science and Technology.

#### REFERENCES

- Alexander, M. A., I. Bladé, M. Newman, J. R. Lanzante, N.-C. Lau, and J. D. Scott, 2002: The atmospheric bridge: The influence of ENSO teleconnections on air–sea interaction over the global oceans. *J. Climate*, **15**, 2205–2231.
- Annamalai, H., P. Liu, and S.-P. Xie, 2005: Southwest Indian Ocean SST variability: Its local effect and remote influence on Asian monsoons. *J. Climate*, **18**, 4150–4167.
- Arai, M., and M. Kimoto, 2008: Simulated interannual variation in summertime atmospheric circulation associated with the East Asian monsoon. *Climate Dyn.*, **31**, 435–447.
- Chang, C.-P., Y. Zhang, and T. Li, 2000: Interannual and interdecadal variations of the East Asian summer monsoon and tropical Pacific SSTs. Part I: Roles of the subtropical ridge. *J. Climate*, **13**, 4310–4325.
- Chowdary, J. S., S.-P. Xie, J.-J. Luo, J. Hafner, S. Behera, Y. Masumoto, and T. Yamagata, 2010: Predictability of Northwest Pacific climate during summer and the role of the tropical Indian Ocean. *Climate Dyn.*, doi:10.1007/s00382-009-0686-5, in press.
- Collins, W. D., and Coauthors, 2006: The Community Climate System Model version 3 (CCSM3). *J. Climate*, **19**, 2122–2143.
- Du, Y., S.-P. Xie, G. Huang, and K. Hu, 2009: Role of air–sea interaction in the long persistence of El Niño–induced north Indian Ocean warming. *J. Climate*, **22**, 2023–2038.
- Gill, A. E., 1980: Some simple solutions for heat-induced tropical circulation. *Quart. J. Roy. Meteor. Soc.*, **106**, 447–462.
- Huang, B., and J. L. Kinter III, 2002: Interannual variability in the tropical Indian Ocean. *J. Geophys. Res.*, **107**, 3319, doi:10.1029/2001JC001278.
- Huang, R., and Y. Wu, 1989: The influence of ENSO on the summer climate change in China and its mechanism. *Adv. Atmos. Sci.*, **6**, 21–32.
- Joseph, P. V., J. K. Eischeid, and R. J. Pyle, 1994: Interannual variability of the onset of the Indian summer monsoon and its association with atmospheric features, El Niño, and sea surface temperature anomalies. *J. Climate*, **7**, 81–105.
- Kalnay, E., and Coauthors, 1996: The NCEP/NCAR 40-Year Reanalysis Project. *Bull. Amer. Meteor. Soc.*, **77**, 437–471.
- Kawamura, R., T. Matsuura, and S. Iizuka, 2001: Role of equatorially asymmetric sea surface temperature anomalies in the Indian Ocean in the Asian summer monsoon and El Niño–Southern Oscillation coupling. *J. Geophys. Res.*, **106**, 4681–4693.
- Klein, S. A., B. J. Soden, and N.-C. Lau, 1999: Remote sea surface temperature variations during ENSO: Evidence for a tropical atmospheric bridge. *J. Climate*, **12**, 917–932.
- Kosaka, Y., and H. Nakamura, 2006: Structure and dynamics of the summertime Pacific Japan teleconnection pattern. *Quart. J. Roy. Meteor. Soc.*, **132**, 2009–2030.
- Kwon, M., J.-G. Jhun, B. Wang, S.-I. An, and J.-S. Kug, 2005: Decadal change in relationship between east Asian and WNP summer monsoons. *Geophys. Res. Lett.*, **32**, L16709, doi:10.1029/2005GL023026.
- Lau, N.-C., and M. J. Nath, 2003: Atmosphere–ocean variations in the Indo-Pacific sector during ENSO episodes. *J. Climate*, **16**, 3–20.
- Li, S., J. Lu, G. Huang, and K. Hu, 2008: Tropical Indian Ocean Basin warming and East Asian summer monsoon: A multiple AGCM study. *J. Climate*, **21**, 6080–6088.
- Lu, R. Y., Y. Li, and B. W. Dong, 2006: External and internal summer atmospheric variability in the western North Pacific and East Asia. *J. Meteor. Soc. Japan*, **84**, 447–462.
- Matsuno, T., 1966: Quasi-geostrophic motions in the equatorial area. *J. Meteor. Soc. Japan*, **44**, 25–43.
- Murakami, T., and J. Matsumoto, 1994: Summer monsoon over the Asian continent and western North Pacific. *J. Meteor. Soc. Japan*, **72**, 719–745.
- Nitta, T., 1987: Convective activities in the tropical western Pacific and their impact on the Northern Hemisphere summer circulation. *J. Meteor. Soc. Japan*, **65**, 373–390.
- Rayner, N. A., D. E. Parker, E. B. Horton, C. K. Folland, L. V. Alexander, D. P. Rowell, E. C. Kent, and A. Kaplan, 2003: Global analyses of sea surface temperature, sea ice, and night marine air temperature since the late nineteenth century. *J. Geophys. Res.*, **108**, 4407, doi:10.1029/2002JD002670.
- Rowell, D. P., C. K. Folland, K. Maskell, and N. M. Ward, 1995: Variability of summer rainfall over tropical north Africa (1906–92): Observations and modelling. *Quart. J. Roy. Meteor. Soc.*, **121**, 669–704.
- Schott, F. A., S.-P. Xie, and J. P. McCreary Jr., 2009: Indian Ocean circulation and climate variability. *Rev. Geophys.*, **47**, RG1002, doi:10.1029/2007RG000245.
- Ueda, H., and T. Yasunari, 1996: Maturing Process of the Summer Monsoon over the Western North Pacific—A Coupled Ocean/Atmosphere System. *J. Meteor. Soc. Japan*, **74**, 493–508.
- , M. Ohba, and S.-P. Xie, 2009: Important factors for the development of the Asian–Northwest Pacific summer monsoon. *J. Climate*, **22**, 649–669.
- Wang, B., R. Wu, and K.-M. Lau, 2001: Interannual variability of the Asian summer monsoon: Contrasts between the Indian and the western North Pacific–East Asian monsoons. *J. Climate*, **14**, 4073–4090.
- , —, and T. Li, 2003: Atmosphere–warm ocean interaction and its impacts on Asian–Australian monsoon variation. *J. Climate*, **16**, 1195–1211.
- , J. Yang, T. Zhou, and B. Wang, 2008: Interdecadal changes in the major modes of Asian–Australian monsoon variability: Strengthening relationship with ENSO since the late 1970s. *J. Climate*, **21**, 1771–1789.

- Wu, R., and B. Wang, 2000: Interannual variability of summer monsoon onset over the western North Pacific and the underlying processes. *J. Climate*, **13**, 2483–2501.
- , B. P. Kirtman, and V. Krishnamurthy, 2008: An asymmetric mode of tropical Indian Ocean rainfall variability in boreal spring. *J. Geophys. Res.*, **113**, D05104, doi:10.1029/2007JD009316.
- Xie, S.-P., and S. G. H. Philander, 1994: A coupled ocean-atmosphere model of relevance to the ITCZ in the eastern Pacific. *Tellus*, **46A**, 340–350.
- , H. Annamalai, F. A. Schott, and J. P. McCreary Jr., 2002: Structure and mechanisms of South Indian Ocean climate variability. *J. Climate*, **15**, 864–878.
- , K. Hu, J. Hafner, H. Tokinaga, Y. Du, G. Huang, and T. Sampe, 2009: Indian Ocean capacitor effect on Indo-western Pacific climate during the summer following El Niño. *J. Climate*, **22**, 730–747.
- , Y. Du, G. Huang, X.-T. Zheng, H. Tokinaga, K. Hu, and Q. Liu, 2010: Decadal shift in El Niño influences on Indo-western Pacific and East Asian climate in the 1970s. *J. Climate*, **23**, 3352–3368.
- Yang, J., Q. Liu, S.-P. Xie, Z. Liu, and L. Wu, 2007: Impact of the Indian Ocean SST basin mode on the Asian summer monsoon. *Geophys. Res. Lett.*, **34**, L02708, doi:10.1029/2006GL028571.